Article

Cell Reports

Regulation of Mesenchymal Stem to Transit-Amplifying Cell Transition in the Continuously Growing Mouse Incisor

Graphical Abstract

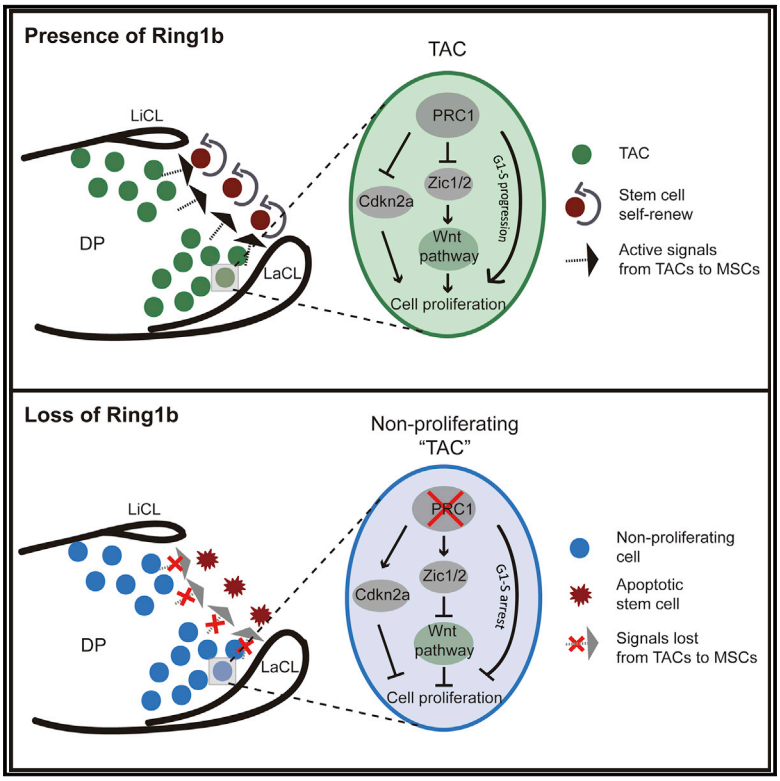

Authors

Zhengwen An, Basem Akily, Maja Sabalic, Guo Zong, Yang Chai, Paul T. Sharpe

Correspondence

paul.sharpe@kcl.ac.uk

In Brief

Using a combination of transcriptomic and epigenomic approaches, An et al. show that polycomb Ring1 in transit-amplifying cells acts as a global regulator by directly inhibiting Cdkn2a and regulating Wnt/β-catenin-signaling activity. Loss of proliferation of TACs results in MSC apoptosis, yielding positive feedback between TACs and mesenchymal stem cells.

Highlights

- Transcriptomic and epigenomic identification of PRC1 targets in TACs
- Control of proliferation by PRC1 via repressing Cdkn2a and activating G1-S genes
- Activation of Wnt signaling in TACs is a main pathway regulated by PRC1
- TACs are required to maintain stem cells

Data and Software Availability

GSE104893
GSE104891
GSE104892
GSE104934

An et al., 2018, Cell Reports *23*, 3102–3111
June 5, 2018
https://doi.org/10.1016/j.celrep.2018.05.001

CellPress

OPEN ACCESS
CellPress

Cell Reports
Article

Regulation of Mesenchymal Stem to Transit-Amplifying Cell Transition in the Continuously Growing Mouse Incisor

Zhengwen An,[1] Basem Akily,[1] Maja Sabalic,[1] Guo Zong,[1] Yang Chai,[2] and Paul T. Sharpe[1,3,*]
[1]Centre for Craniofacial and Regenerative Biology, Dental Institute, Kings College, London, UK
[2]Center for Craniofacial Molecular Biology, University of Southern California, Los Angeles, CA, USA
[3]Lead Contact
*Correspondence: paul.sharpe@kcl.ac.uk
https://doi.org/10.1016/j.celrep.2018.05.001

SUMMARY

In adult tissues and organs with high turnover rates, the generation of transit-amplifying cell (TAC) populations from self-renewing stem cells drives cell replacement. The role of stem cells is to provide a renewable source of cells that give rise to TACs to provide the cell numbers that are necessary for cell differentiation. Regulation of the formation of TACs is thus fundamental to controlling cell replacement. Here, we analyze the properties of a population of mesenchymal TACs in the continuously growing mouse incisor to identify key components of the molecular regulation that drives proliferation. We show that the polycomb repressive complex 1 acts as a global regulator of the TAC phenotype by its direct action on the expression of key cell-cycle regulatory genes and by regulating Wnt/β-catenin-signaling activity. We also identify an essential requirement for TACs in maintaining mesenchymal stem cells, which is indicative of a positive feedback mechanism.

INTRODUCTION

The continuously growing mouse incisor is increasingly studied as a model to investigate the organization of adult mesenchymal stem cell (MSC) niches (An et al., 2018; Sharpe, 2016; Yu et al., 2015). The self-sharpening action at the tips of opposing incisors resulting from their occlusion results in the continuous loss of cells (Pang et al., 2016). These cells are continuously replaced by the activity of stem cell populations located at the proximal end of the incisor. The directional growth of the incisor means that the stem cells and their progeny (transit-amplifying cells) have clearly defined positions along the proximodistal axis, and thus cell conversions and interactions can be studied easily. A population of slow-cycling, Shh-responsive mesenchymal stem cells occupies an area of dental pulp in the proximal core of the incisors between the epithelial cervical loops, which can be identified as $Gli1^{+}$ cells (Zhao et al., 2014). These MSCs give rise to a spatially distinct transit-amplifying cell (TAC) population of rapidly proliferating cells that differentiate into the main specialized tooth-specific cell type, odontoblasts, and the fibroblastic pulp cells. Odontoblasts are required for the formation of the main mineralized tissue of the tooth, the dentin.

The MSCs reside in a neurovascular bundle at the proximal end of the incisor from which they receive Shh signals required for their maintenance (Zhao et al., 2014). Genetic lineage tracing has established that both neuronal glial cells and pericytes act as sources of these MSCs (Feng et al., 2010, 2011; Kaukua et al., 2014). Distal to the MSCs, the TACs continuously form odontoblasts and pulp cells, although because TACs are pulp cells themselves, it is unclear whether this is an active or a passive differentiation process. Odontoblasts form around the periphery of the incisor and the spatial location of individual MSCs, and their TAC progeny determines the relative contributions to odontoblast and/or pulp cell differentiation (Kaukua et al., 2014). In addition to their high proliferation rate, TACs can be distinguished by the expression of the components of the polycomb repressive complex 1 (PRC1) that are required to maintain TAC proliferation (Lapthanasupkul et al., 2012).

In adulthood, a state of growth homeostasis is achieved by the rate of transition of MSCs to TACs and the subsequent rate of TAC proliferation and differentiation. The transition from a slow-cycling, self-renewing, non-differentiating stem cell into a fast-cycling, non-self-renewing, differentiating progenitor cell phenotype (TAC) must be a highly regulated process but one that is poorly understood. In addition, the extent to which there is feedback communication between TACs and MSCs to maintain the rate of MSC-TAC conversion is unknown.

Using a combination of transcriptomic and epigenomic approaches, we show here that expression of components of PRC1 in TACs regulates their proliferation by directly inhibiting the cell-cycle inhibitor Cdkn2a and activating the expression of positive cell-cycle regulators such as cyclin E2, Cdc6, and Cdc45. The transition from slow to fast cycling is enhanced further by the Wnt/β-catenin-signaling pathway, which is elevated in TACs by the action of members of the Zic family of transcription factors that also are regulated directly by PRC1. Finally, we show that loss of proliferation of the TAC population results in the rapid loss of MSCs as a result of apoptosis, identifying a positive feedback mechanism of communication between TACs and MSCs.

RESULTS

Ring1b Expression Co-localizes with TACs

Ring1b expression has been shown to be localized in the region of mesenchymal cells, with the highest rates of proliferation in the mouse incisor, and its targeted deletion resulted in the loss of TAC proliferation and arrest of incisor growth (Lapthanasupkul et al., 2012). To visualize different cell proliferation rates in the incisor, we used nucleoside analog (5-ethynyl-2′-deoxyuridine [EdU]) incorporation to identify the TACs (Figures 1A and S1) as being distal to the slow-cycling MSCs (Figure 1B). TACs were identified as EdU^+ cells chased for 16 to 24 hr, while slow-cycling cells were EdU labeled for 4 weeks followed by chasing for another 2 to 6 months. Fluorescence-activated cell sorting (FACS) analysis of EdU^+ cells identified approximately 16% of total pulp cells as TACs (Figure 1A) and 2.5% as slowcycling MSCs (Figure 1B). Using immunohistochemistry on sections of incisors from mice that had received EdU 24 hr previously, we established that rapidly proliferating cells (TACs) co-localize with Ring1b protein (Figures 1C–1G). Co-immunolocalization for slow-cycling label-retaining stem cells and Ring1b protein confirmed the location of Ring1b as being TACs and absent from the stem cells (Figures 1H–1K). Finally, to confirm the effect of the loss of Ring1 proteins on cell proliferation, we stained sections for Ki67 protein. In controls, Ki67 co-localized in the same region as Edu^+ cells, but in $Ring1a^{-/-};Ring1b^{cko/cko}$ incisors, $Ki67^+$ cells were barely detectable (Figure 1L), as shown previously (Lapthanasupkul et al., 2012). Ring1b protein is thus specifically localized in the rapidly proliferating MSCs of the incisor, just distal to the location of the slow-cycling MSCs.

Genome-wide Analysis of PRC1 in TACs

To gain a genome-wide view of PRC1 components in TACs, we used FACS-sorted TACs and carried out low-input chromatin immunoprecipitation sequencing (ChIP-seq) with Ring1b antibodies in addition to H3K4me3 and H3K27me3 histone codes to determine the active and repressive regions regulated by Ring1. Peak calling on H3K4me3, H3K27me3, and Ring1b ChIP-seq, identified 14,361, 11,341, and 3,938 gene loci, respectively (Figure 2A). A total of 2,624 gene loci were co-marked by H3K4me3 and Ring1b, whereas 1,591 loci were marked with H3K27me3 and Ring1b. Representative genome browser snapshots of repressed and active genes are shown in Figure 2B. Heatmaps were generated to determine active region distribution across targets on H3K4me3 and H3K27me3 ChIP-seq via bigWIG metrics and defined as five clusters, C1–C5 (Figure 2C). C1, C4, and C5 groups are gene loci bound by H3K4me3 at the transcription start site (TSS), 500 bp downstream and 1 kb upstream of the TSS, respectively. C2 is a group bound by H3K4me3 only, and group C3 shows no difference between H3K4me3 and H3K27me3.

Hox genes are known targets of PRC1 (Elderkin et al., 2007; Eskeland et al., 2010; Suzuki et al., 2002), and our ChIP-seq data identified a number of Hox genes occupying the same loci as Ring1b with H3K27me3 but no enrichment with H3K4me3 (Figure S2). Peak calling on H3K4me3 revealed PRC1 component genomic distribution in TACs. Genome browser snapshots showed enriched peaks of Ring1a, Ring1b, Cbx2, and Pcgf1/2 at gene promoter regions on H3K4me3 ChIP but no enrichment on H3K27me3 ChIP (Figure 2D). To identify the protein-protein co-localization, we collected flow-sorted EdU^+ cells (TACs) and carried out immunofluorescence with Ring1b and Cbx2. We found co-localization of Ring1b and Cbx2 in TACs (Figures 2E–2G and S3). Based on the role of PRC1 in chromatin modification, we performed co-immunoprecipitation and identified a Ring1b interaction with H3K27me3 but not with H2AK119ub (Figure 2H). Conditional knockout of Ring1b decreased trimethylation levels of H3K27 as revealed by western blots (Figure 2I). These results demonstrate that the PRC1 complex in TACs comprises Ring1b, Cbx2, and Pcgf1/2 and has a repressive role via trimethylation of H3K27 rather than monoubiquitination on H2AK119.

Linking Gene Expression to PRC Binding and Histone Codes Identifies Cell-Cycle Regulation

Given that knock out of Ring1 decreases cell proliferation (Figure 1D) (Lapthanasupkul et al., 2012), we used whole-genome microarrays to compare gene expression between $Ring1^+$ and $Ring1^-$ incisor pulp mesenchymal cells. Volcano plots revealed that 499 genes increased by >2-fold ($p < 0.05$) and 466 decreased (Figure 3A; Table S1). Principal component analysis (PCA) confirmed and grouped the samples by similarities and differences. As visualized in the PCA plot, the control samples clustered separately from the Ring1 deletion samples (Figure 3B). Hierarchical clustering of samples showed the genes differentially expressed upon Ring1 deletion and included a number of Hox genes and cell-cycle inhibitors as upregulated (Figures 3C and S4; Table S1). We carried out detailed Gene Ontology, *Kyoto Encyclopedia of Genes and Genomes* (KEGG), and WiKiPathways analyses of downregulated genes that revealed the top five pathways to be related to cell proliferation (Figure 3D). These results demonstrated that Ring1b likely acts as a cell-cycle regulator during homeostasis in the continuously growing mouse incisor.

Because the defining feature of TACs is their high rate of proliferation, we focused on the epigenomic status of key cell-cycle regulatory genes. We further validated four of the positive cell-cycle regulators, cyclin E2, Cdc45, Cdc6, and Cdc7, as genes involved in G1-S control and DNA replication and found to be downregulated upon Ring1 deletion (Figures 3E and 3I; Table S2). These gene loci also were recognized by Ring1b and H3K4me3 but not by H3K27me3 in ChIP-seq datasets (Figure 3F). We next analyzed the upregulated genes via heatmaps and dot plots and identified the elevated expression of Cdkn2a, a major negative cell-cycle regulator from the microarray analysis (Figure 3G). ChIP-seq identified Cdkn2a as a direct target of Ring1b marked by H3K27me3 bound across the entire gene locus (Figure 3H). This overall pattern was consistent for all positive and negative cell-cycle regulatory genes in microarrays and ChIP-seq data, because all of them were found bound by Ring1b. Real-time PCR confirmed the downregulated G1-S control genes and the upregulated cell-cycle inhibitor Cdkn2a following depletion of Ring1 (Figure 3J; Table S2). Loss of Ring1 function thus has major effects on gene expression in incisor mesenchymal cells. Genes that positively regulate the

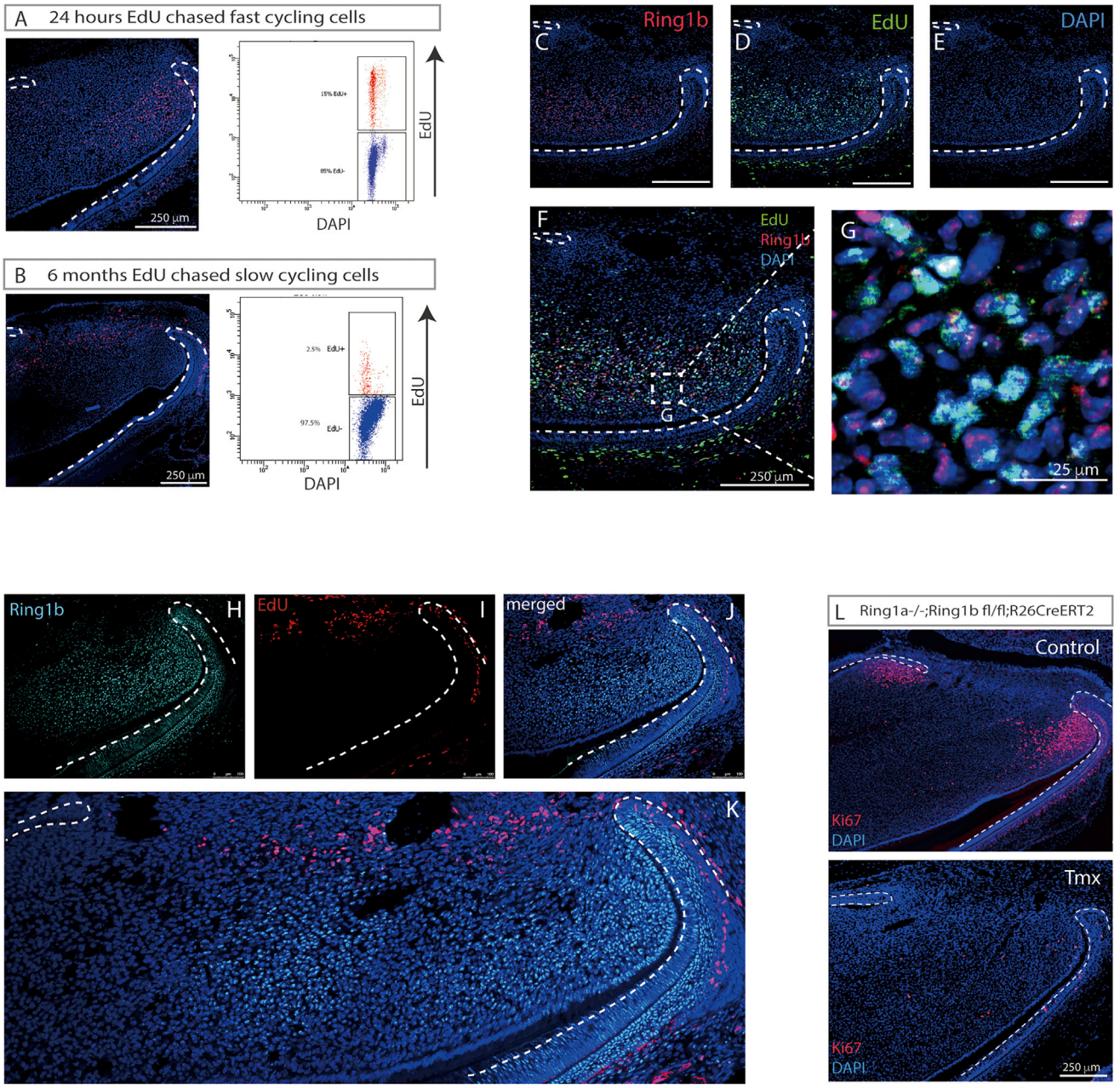

Figure 1. MSC Niche in the Mouse Incisor

(A and B) To label fast-cycling cells (TACs), postnatal day 5 pups were given a single EdU injection (3.3 μg/g BW) and sacrificed after 16–24 hr (A). To identify slow-cycling cells, postnatal day 5 pups were given daily EdU injections (3.3 μg/g BW) for 4 weeks and traced for 2–6 months before tissue collection (B). Click-it EdU image kit was used for EdU detection on sagittal sections of mouse incisors. EdU was labeled with Alexa Fluor 594 dye and DAPI was used for nuclear labeling.

(C–G) Immunofluorescence showed that Ring1b (C) co-localized with EdU-labeled TACs (D) in dental mesenchyme (82% EdU^+ are $Ring1b^+$, and 70% $Ring1b^+$ are EdU^+). DAPi staining (E), merged image (F), and (G) Enlarged field of (F) showing localization of Ring1b and EdU^+ in the TAC region.

(H–K) Immunolocalization of Ring1b (H) and slow-cycling (label-retaining) cells (I).

(J) Merged image.

(K) Tilescan image of (J).

(L) Loss of Ring1a/b showed decreased cell proliferation identified by Ki67 staining.

N ≥ 3 mice per group.

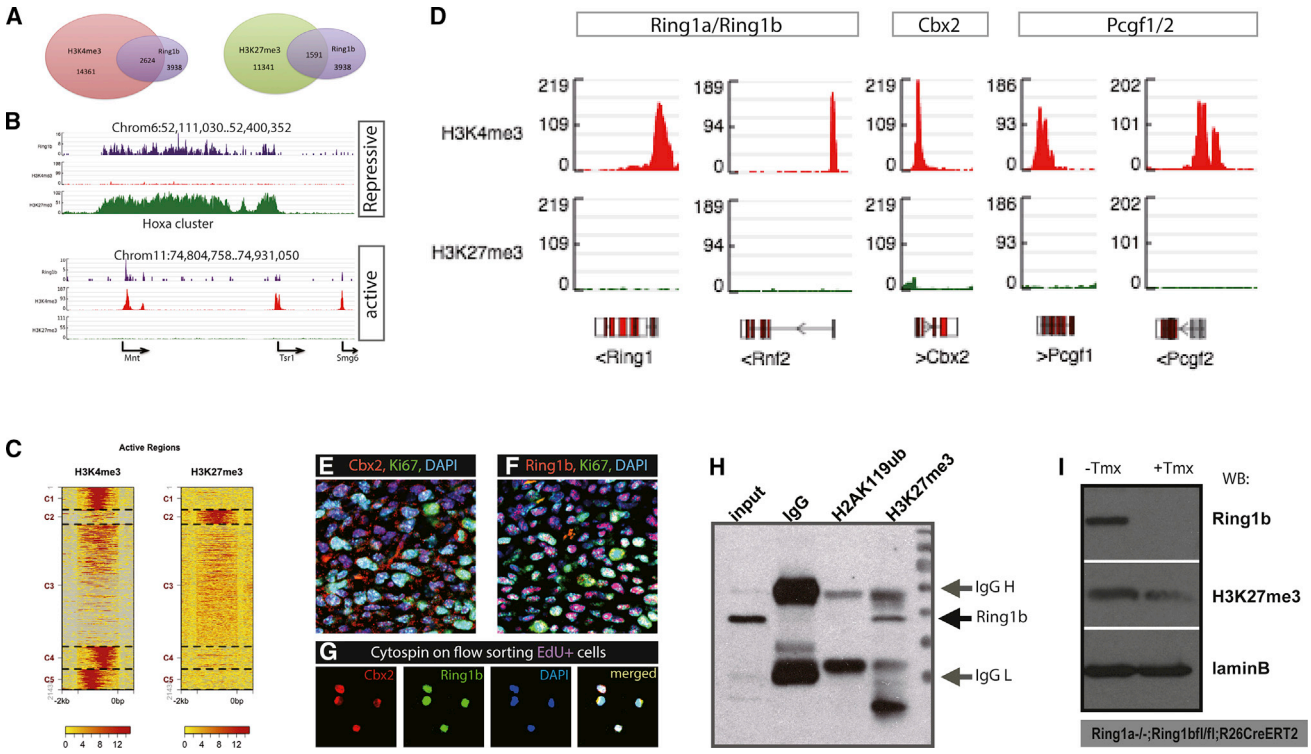

Figure 2. Genome-wide Landscapes of PRC1 in TACs

(A) ChIP-seq on Ring1b, H3K4me3, and H3K27me3 identified 3,939, 14,361, and 11,341 gene loci, respectively. There were 2,624 gene loci co-occupied by both H3K4me3 and Ring1b, whereas 1,591 loci were marked with H3K27me3 and Ring1b.

(B) Genome browser snapshots representing repressive and active gene loci regulated by Ring1b.

(C) BigWIG metrics identified five clusters across targets in H3K4me3 and H3K27me3 active regions.

(D) Snapshots of genome browser showed the enrichment of PRC1 components in TACs.

(E and F) Double immunolocalization of Ki67 (E) with Cbx2 and Ring1b (F), respectively, in the TAC region.

(G) Flow-sorted EdU^{+} fast-cycling cells were collected by cytospin and immunofluorescence staining showed co-localization of Ring1b and Cbx2 on EdU^{+} cells.

(H) Co-immunoprecipitation with H2AK119ub1 and H3K27me27 on primary dental pulp cells by Ring1b antibody identified interaction of Ring1b and H3K27m3 rather than H2AK119ub1.

(I) Conditional knock out of Ring1b caused decreased levels of H3K27me3 demonstrated by western blots. Lamin B antibody was used as an internal loading control.

N $\geq$ 5 mice per group.

cell cycle were downregulated, whereas a major negative regulator was upregulated.

Identification of the Wnt/β-Catenin Pathway in TACs

The microarray analysis revealed downregulation of Wnt/β-catenin pathway genes in TACs following the loss of Ring1 function (Figure 3D). To investigate this further, we mined the ChIP-seq datasets for cell-signaling pathways using Protein Analysis Through Evolutionary Relationships (PANTHER) (Mi et al., 2013). GO enrichment analysis showed that Wnt/β-catenin signaling emerged as the top pathway hit on both Ring1b (Figure 4A) and H3K4me3 datasets (Figure 4B). Wnt target genes such as Axin2, β-catenin, cyclin D1, cMyc, E2f1, and Twist1 showed peaks co-occupied by H3K4me3 and Ring1b but not by H3K27me3 in ChIP-seq (Figure 4C). qPCR confirmed the downregulation of Wnt targets by Ring1 deletion (Figure 4D). Zic genes code for transcriptional repressors of Wnt signaling activity and are repressed in cells where Wnt pathway genes are active (Chiacchiera et al., 2016). The H3K27me3 dataset identified Zic1/2 genes as bound loci that also were bound by Ring1b (Figure 4E), which is consistent with Wnt-signaling activity in TACs being regulated by Ring1. Further support for this role came from qPCR of Ring1b$^{-/-}$ pulp cells that showed dramatically increased expression of Zic1 and Zic2 (Figures 4F and S4; Table S2). Ring1 is thus bound at loci of both Wnt-signaling pathway active genes and Wnt-signaling pathway repressor genes in combination with either H3K4me3 or H3K27me3, respectively.

Wnt/β-Catenin Pathway *In Vivo*

To confirm the status of Wnt/β-catenin-signaling activity in TACs *in vivo*, we used Axin2^{LacZ} mice (van Amerongen et al., 2012). Maximum levels of Axin2 expression (Figure S5) were localized in the regions occupied by TACs (Figure S5) and was expressed in odontoblasts. Little Axin2 expression could be visualized in stem cells, as has been suggested from TOPGal staining (Yang et al., 2015). To confirm this location, we used genetic lineage tracing of Axin2-expressing cells with

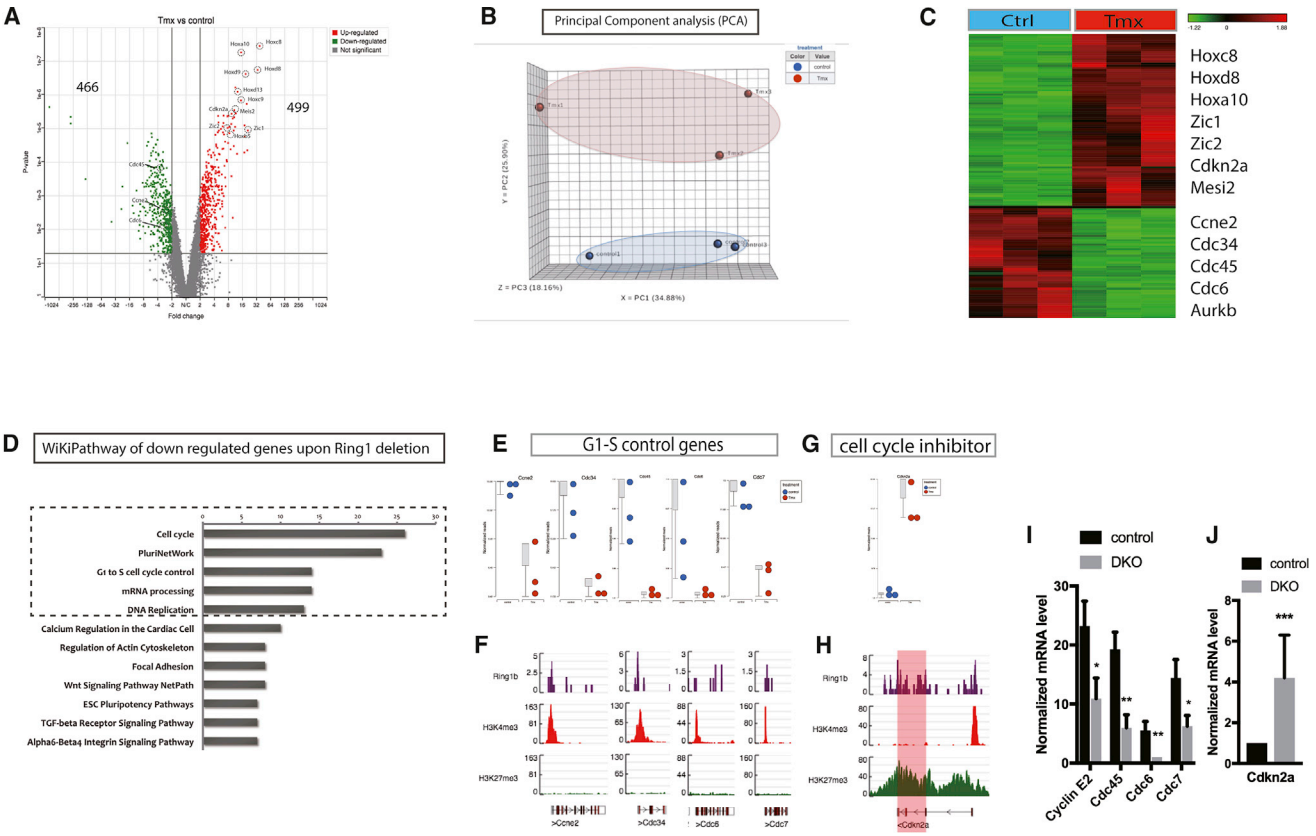

Figure 3. Gene Expression and ChIP-Seq Identify the Role of PRC1 on Cell-Cycle Regulation

(A) Whole-genome microarrays revealed that 499 genes were upregulated and 466 genes were downregulated with >2-fold change ($p < 0.05$) upon Ring1a/b deletion represented by volcano plots.

(B) PCA plots identified and grouped the samples by similarities and differences.

(C) Heatmaps representing hierarchical clustering of differentially expressed genes following loss of Ring1a/b (n = 3 biological replicates, minimum four mice per group).

(D) WiKiPathway revealed the top five pathways to be related to cell-cycle regulation.

(E) G1-S control and DNA replication genes were found downregulated upon Ring1 deletion on gene microarray datasets and (F) the enrichment loci also were co-marked by Ring1b and H3K4me3 but not with H3K27me3 on ChIP-seq datasets.

(G) Cell-cycle inhibitor Cdkn2a was found to be upregulated in Ring1b^{-} cells and (H) identified as a direct target of Ring1b marked by H3K27me3. A single peak of H3K4me3 is present upstream of the Cdkn2a start site in a region also bound by H3K27me3. Highlighted region shows the gene transcription region for Cdkn2a.

(I and J) Real-time PCR confirmed the (I) upregulated cell-cycle genes and downregulation (J) of Cdkn2a upon Ring1 deletion in mouse dental pulp cells.

N ≥ 3 mice per group. *$p < 0.05$, **$p < 0.01$, and ***$p < 0.001$ by Student's t test. Data presented as means ± SEMs.

Axin2^{ERT2cre};Rosa26R$^{mt/mg}$ reporter mice. Immediately following tamoxifen induction, GFP^{+} cells were seen in the odontoblast layer (odontoblasts express Axin2) and pulp cells in the proximal region (Figure 5). At later time points post-tamoxifen, GFP^{+} cells became progressively more distally located, and by 30 days, all GFP^{+} cells have disappeared. Thus, Axin2^{+} cells are located in the TAC zone and give rise to pulp cells that show a temporal proximal-distal progression. These labeled cells are removed at the tips during growth and are not continuously replaced by new labeled cells. Axin2^{+} cells, therefore, correspond to a population of rapid-cycling, non-self-renewing cells, consistent with a TAC identity (Figure 5).

TACs Are Required for Stem Cell Maintenance

We hypothesized that the loss of cell proliferation in the TAC zone as a result of the loss of Ring1 function also may indirectly affect the stem cells because TAC numbers and stem cell division must be interlinked in some way. Using the nucleoside retention to detect the slow-cycling stem cells (Figure 6A), we observed that EdU^{+} cells were barely detectable 96 hr post-tamoxifen induction of Ring1b deletion on a Ring1a$^{-/-}$ background compared with controls (Figure 6B). Tunel assays showed that whereas few apoptotic cells were present in the stem cell zone before tamoxifen administration, 96 hr after administration (Ring1b$^{cko/cko}$;Ring1a$^{-/-}$), a line of apoptotic cells corresponding to the location of slow-cycling stem cells was observed (Figure 6C). Significantly, no increase in apoptotic cells was observed in the TAC zone or elsewhere in the incisor (Figure 6C). Because Wnt signaling activity is localized to TACs, we investigated the impact of blocking Wnt activity in TACs. Gpr177 codes for the Wntless protein that is required for the secretion of Wnt ligands (Carpenter et al., 2010). We generated

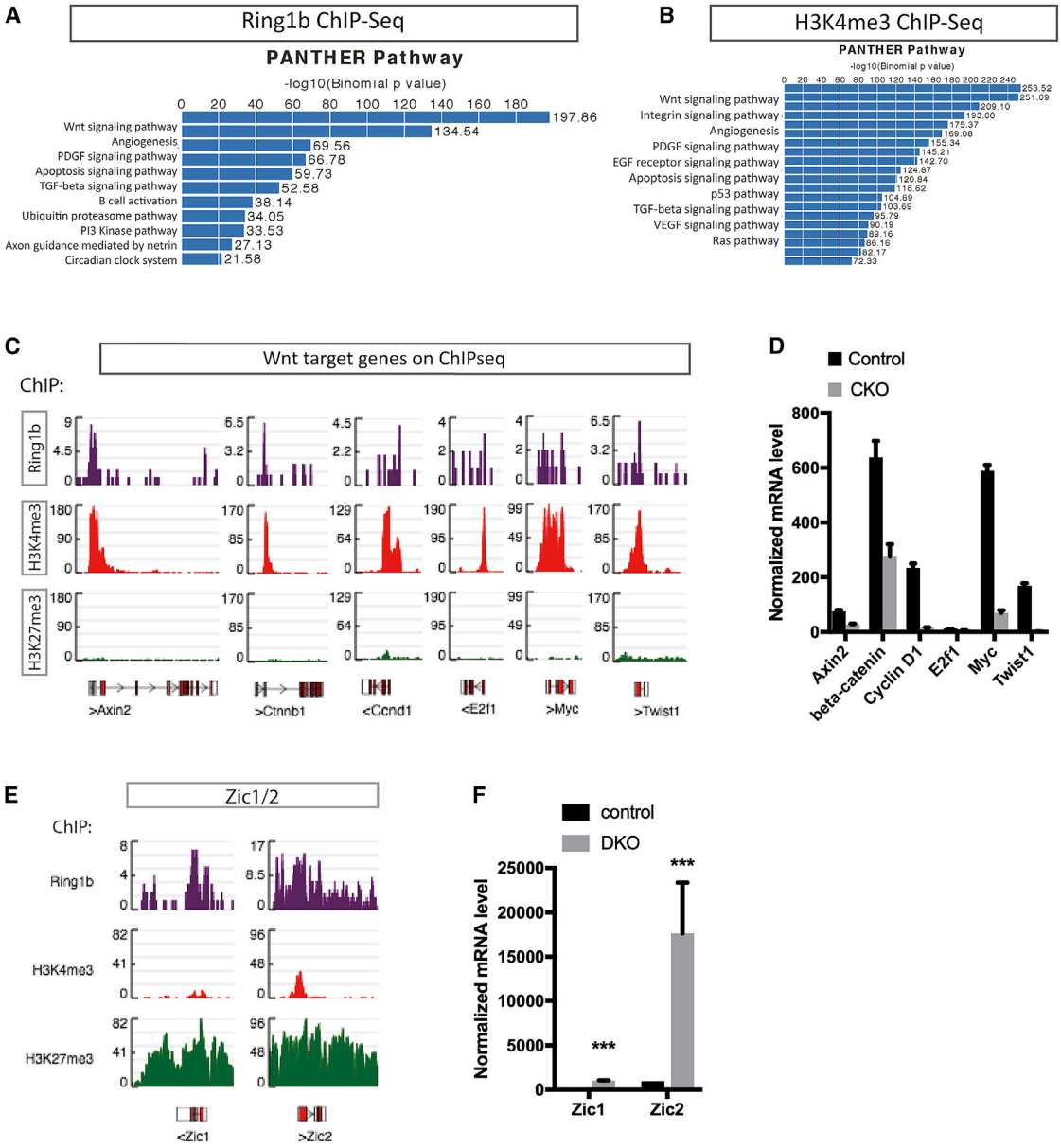

Figure 4. ChIP-Seq Analysis Reveals Ring1b Targets in the Wnt Pathway

(A and B) GO enrichment analysis using PANTHER pathway identified Wnt/β-catenin signaling as the top pathway in Ring1b (A) and H3K4me3 (B) ChIP-seq datasets.

(C) Peak calling showed the enrichment of Wnt target genes co-marked by Ring1b and H3K4me3 but no enrichment with H3K27me3.

(D) Validation of downregulated Wnt target genes by Ring1b using real-time PCR. N ≥ 3 mice per group. $p < 0.05$ by Student's t test. Data presented as means ± SEMs.

(E) Genomic view of Zic1/2 co-occupying the same loci as Ring1b and H3K27me3 rather than H3K4me3.

(F) Zic1/2 were upregulated following deletion of Ring1a/b identified by real-time PCR.

N ≥ 3 mice per group. ***$p < 0.001$ by Student's t test. Data presented as means ± SEMs.

Wntless conditional mutant mice using $Wls^{flox/flox}$ crossed with $Axin2^{ERT2cre}$ and administered tamoxifen to adult animals. Seven days post-tamoxifen, cell proliferation in TACs detected by nucleoside incorporation was substantially reduced, as was the rate of incisor growth (Figures 6D and S5C). Using the early apoptosis marker, annexin V, we identified apototic cells exclusively in the stem cell zone 2 days post-tamoxifen following Ring1-targeted deletion in TACs ($Axin2^{ERT2cre}$) (Figure 6E). Loss of Wnt activity in TACs thus phenocopies the loss of Ring1 function showing reduced proliferation and stem cell apoptosis.

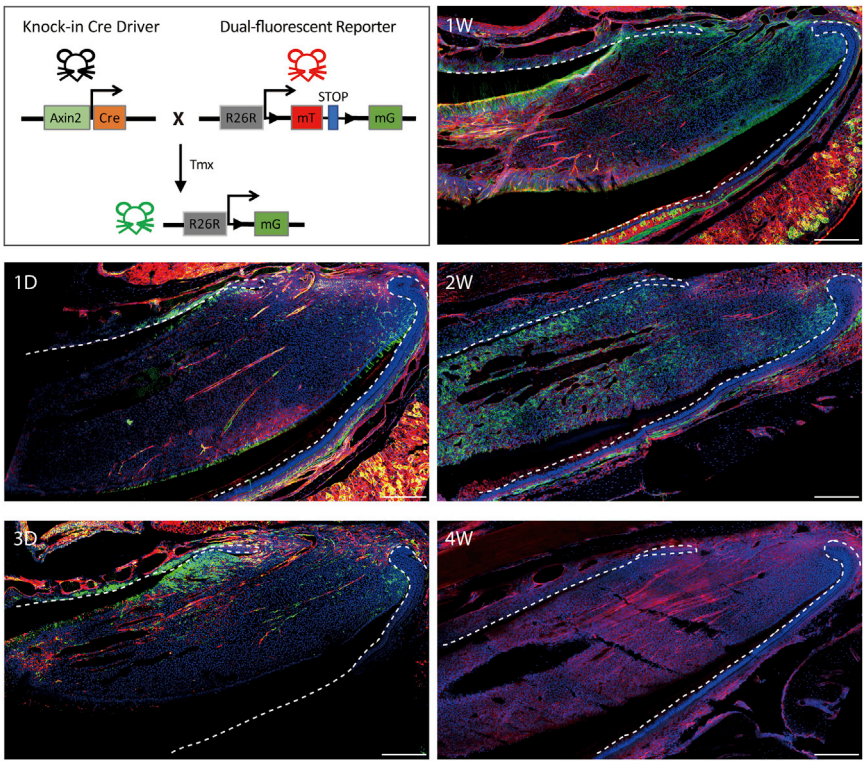

Figure 5. Wnt Signals in the MSC Niche

Lineage tracing of Axin2 progeny (GFP$^+$) at 1 day, 3 days, 1 week, 2 weeks, and 4 weeks post-tamoxifen injection of Axin2^{ERT2cre};mTmG mice on sagittal sections of mouse incisors. GFP$^+$ cells were detected in the TAC region of dental mesenchyme close to the epithelial cervical loop after 1 day and increased in number by 3 days post-tamoxifen. Axin2-derived cells (GFP$^+$) showed an increased contribution to dental pulp cells and odontoblasts toward the apical end by 1 week and progressively advanced toward the tip of the incisor by 2 weeks post-tamoxifen. There were no GFP$^+$ cells detected in the mouse incisor after 4 weeks post-tamoxifen. Green is GFP$^+$, red is Tomato$^+$, and blue is DAPI for nuclear staining. N $\geq$ 3 mice per group. Scale bar: 250 μm.

DISCUSSION

The continuously growing mouse incisor provides a model for studying stem cell functions in growth homeostasis. The extremely rapid growth (500–600 μm/day) (Smith and Warshawsky, 1975) and the distinct anatomical locations of the stem cell compartments enables cell interactions to be studied *in vivo* (An et al., 2018; Feng et al., 2011; Juuri et al., 2012; Kaukua et al., 2014; Lapthanasupkul et al., 2012; Seidel et al., 2010; Wang et al., 2007; Zhao et al., 2014). Nucleoside incorporation identifies spatially distinct populations of slow- and fast-cycling cells at the proximal end of the tooth. The slow-cycling cells are Shh responsive, and lineage tracing using Gli1Ert2cre confirms these cells to be stem cells (Zhao et al., 2014). A distally adjacent population of fast-cycling cells are progenitors (TACs) that differentiate into the specialized mesenchymal cells of the tooth, the odontoblasts that form dentin, and the fibroblastic pulp cells.

The transition from slow-cycling, self-renewing stem cells to fast-cycling, non-self-renewing TACs that differentiate into tooth mesenchymal cells is pivotal in controlling the growth rate of the incisor. Whereas genetic lineage tracing has identified the stem cells as Gli1$^+$ cells occupying a neurovascular niche, less is known about the TACs and how their proliferation is activated. We had identified components of the PRC1 complex as being expressed in the TACs and shown that deletion of the core complex component Ring1 resulted in a loss of TAC proliferation (Lapthanasupkul et al., 2012). Functional PRC1 is thus required for TAC proliferation and incisor growth, but its function in controlling proliferation was not understood. We describe here the application of gene expression comparisons and ChIP-seq analysis to identify PRC1 target loci in TACs and correlate these with changes in gene expression following the loss of Ring1. We find that Ring1 co-localizes with Cbx2 in TACs and with H3K27me3 but not H2AK119ub in immunoprecipitations, suggesting a repressive role for PRC1 via association with trimethylation on H3K27 rather than monoubiquitination on H2AK119. Cbx2 shows preference for H3K27me3, whereas Cbx4 and Cbx7 chromatin domains exhibit preference for H3K9me3 (Bernstein et al., 2006; Kaustov et al., 2011; Tardat et al., 2015), and almost no affinity for Cbx6 and Cbx8 for H3K27me3 (Bernstein et al., 2006; Kaustov et al., 2011). Previous ChIP-seq data revealed that PRC1 target domains are broadly or sharply localized with H3K27me3 (Ku et al., 2008), which also was identified by our ChIP-seq datasets. Likewise, our results further suggested that a repressive mechanism of PRC1 in TACs is via Cbx2 association with H3K27me3 independent of histone H2A modification.

There were 2,624 loci identified that bound both Ring1b and H3K4me3, a gene transcription activation mark. Among these Ring 1b/H3K4me3-bound loci were a number of positive regulators of the cell cycle, whereasloci bound by Ring1b and H3K27me3 included major cell-cycle inhibitors such as Cdkn2a, a known direct target of PRC1 (Biehs et al., 2013; Dietrich et al., 2007). Microarrays comparing gene expression between Ring1b$^+$ and Ring1b$^-$ pulp cells showed a decrease in positive cell-cycle-regulator expression following Ring1a/b deletion and a significant increase in Cdkn2a expression. These results suggest that the cell cycle is dually regulated by PRC1 through activating positive cell-cycle regulators and repressing negative regulators.

Identification of the range of expression levels at PRC1 targets by ChIP-seq suggests that PRC1 does not act as an absolute repressor, but it may regulate the extent of RNA polymerase II (RNAPII) transcriptional activity (Brookes et al., 2012; Enderle et al., 2011; Schwartz and Pirrotta, 2008). Studies have highlighted the opposite scenario of polycomb group (PcG) complexes as activators of gene transcription (Aranda et al., 2015;

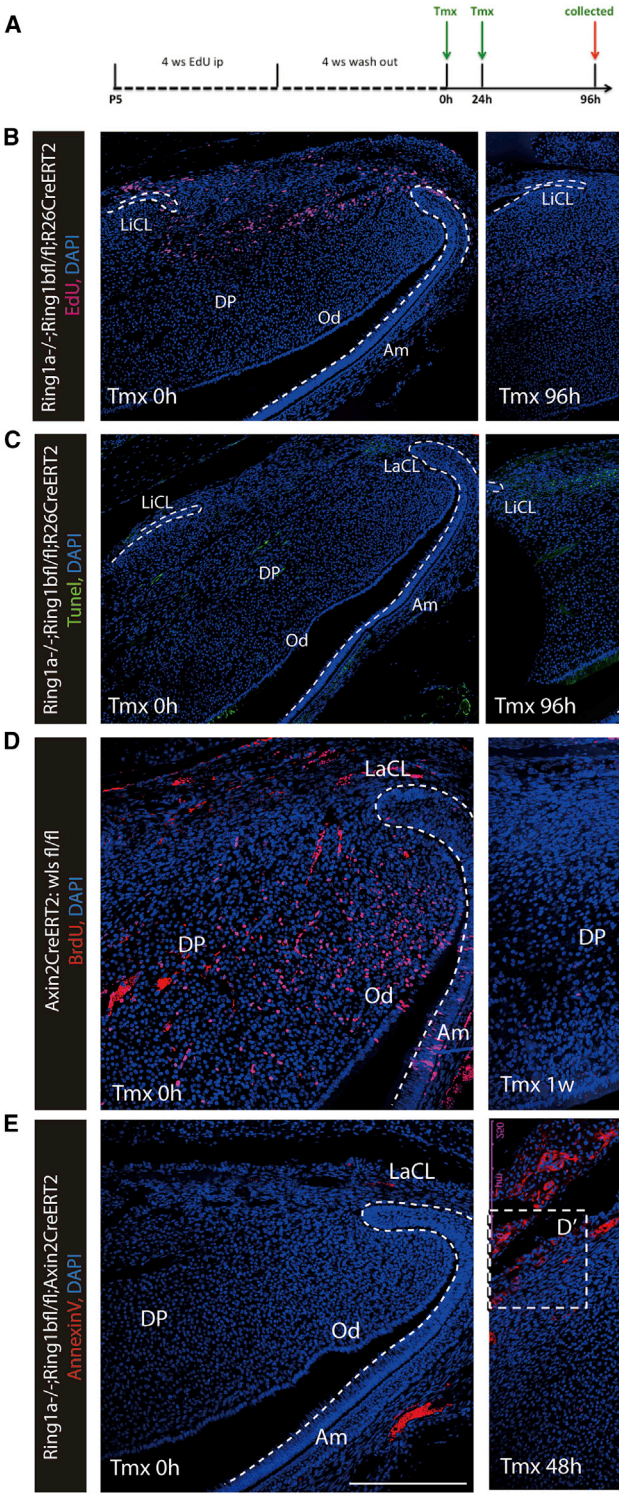

Figure 6. Maintenance of Stem Cell Stability by PRC1

(A) Schematic illustration demonstrated EdU retention assay to detect slow-cycling stem cells.

(B) EdU^{+} cells were distinctly localized between the labial and lingual aspects of the cervical loop, but they disappeared by 96 hr post-tamoxifen induction of Ring1 deletion.

(C) Tunel assays revealed apoptotic cells in the stem cell zone in Ring1^{-} cells, whereas no obvious apoptosis was detected in control incisors.

(D) Reduced cell proliferation was detected in Wls$^{flox/flox}$;Axin2^{CreERT2} marked by BrdU-labeled cells.

(E) Annexin V^{+} apoptotic cells were visible in the stem cell zone 2 days post-tamoxifen on Ring1a$^{-/-}$;Ring1b$^{flox/flox}$;Axin2^{CreERT2} mice compared to controls.

N $\geq$ 3 mice per group.

Frangini et al., 2013; Gao et al., 2014) under different cellular contexts. For example, PRC1 co-occupies active target genes with the Aurora B kinase (Frangini et al., 2013); CK2 protein phosphorylates Ring1B at serine 168 (Gao et al., 2014) and regulates the local topological interaction with Meis2, which binds to a tissue-specific enhancer involved in removing PRC1 from the promoter (Kondo et al., 2014). Aurora B kinase is present in mouse dental pulp mesenchyme and is localized to the TAC region (Figure S6; Table S3), which is the same expression region as Ring1b and may explain the role of PRC1 on transcriptional activation for controlling some positive cell-cycle regulators in TACs.

The main signaling pathway identified from the Ring1/H3K4me3 ChIP-seq datasets was Wnt/β-catenin. The Wnt/β-catenin pathway is involved in the control of cell proliferation, stem cell self-renewal, and cell fate specification, and is associated with several diseases (Clevers, 2006; Clevers and Nusse, 2012; Moon et al., 2004; Reya and Clevers, 2005) Wnt signaling can either stimulate or restrain the process of apoptosis, according to specific cellular environment contexts (Brocardo and Henderson, 2008; Pećina-Slaus, 2010; Yeo and Gautier, 2004). Through the inhibition of Zic transcription factors, PRC1 sustains Wnt/β-catenin activity and preserves adult stem cell identities (Chiacchiera et al., 2016). Our results identify the co-occupied binding loci of Zic1/2 and Wnt target genes by Ring1b. Loss of Ring1b causes the upregulation of Zic1/2 and the downregulation of Wnt signals, indicating that PRC1 regulates the Wnt signaling pathway by repressing Zic1/2 transcription factors.

Depletion of Ring1b decreased cell proliferation in TACs and, surprisingly, caused specific apoptosis of the stem cells. We assume that TACs act as a supportive environment for stem

cell maintenance and hypothesize that secreted signaling proteins produced by TACs act as positive regulators on the adjacent stem cell population. Loss of Wnt signaling also resulted in the apoptosis of stem cells, indicating that Wnt/β-catenin activity downstream of PRC1 is required for stem cell maintenance.

EXPERIMENTAL PROCEDURES

EdU/BrdU Incorporation and Staining

To label fast-cycling cells, mice were intraperitoneally (IP) injected with one dose of EdU (3.3 μg/g body weight) or 5-bromo-2′-deoxyuridine (BrdU) (100 mg/kg body weight) and sacrificed after 16–24 hr. For slow-cycling cell labeling, pups post-natal days 2–5 were IP injected with EdU daily for 4 weeks and chased for another 4 weeks to 6 months before tissue collection. See the Supplemental Experimental Procedures for details.

Flow Cytometry

Mouse incisor pulp tissue was freshly dissected and dissociated as a single cell suspension by TrypLE Express Enzyme (Thermo Fisher Scientific, catalog no. 12604013). Cells were then fixed and stained by Click-iT EdU Alexa Fluor 647 Flow Cytometry Assay kit (Invitrogen, catalog no. C10424), according to the protocol before being subjected to flow cytometry. FACS analysis was carried out on a BD Fortessa cell analyzer and data were analyzed by BD FACSDiva 6.1.3 (both BD Biosciences) or FlowJo software.

ChIP-Seq

See the Supplemental Experimental Procedures for details. Basically, 75-nucleotide sequence reads generated by Illumina sequencing (NextSeq500) were mapped to the mouse genome (mm10 assembly) using the Burrows-Wheeler Aligner (BWA) algorithm. The resulting BAM files were then analyzed, and peak calling used model-based analysis of ChIP-seq (MACS) (Zhang et al., 2008) to identify genomic regions enriched in the proteins in comparison to the total genomic input DNA. Histone ChIPs were analyzed with Spatial Clustering for Identification of ChIP-Enriched Regions (SICER) (Zang et al., 2009).

Gene Microarray

Biological triplicates were processed separately through the entire microarray procedure. Total RNA was extracted using miRNeasy Mini Kits (Qiagen, catalog no. 217004), and cDNA was synthesized using standard Affymetrix protocols. Samples were hybridized to Affymetrix GeneChip Mouse Genome 430 2.0 Arrays. CEL files were generated and then analyzed using Partek Flow pipelines. Reads were aligned with BWA and quantified to the annotation model (Partek E/M). Data were normalized, and genes were analyzed using differential gene expression (GSA) algorithm.

Mice Information

All of the animal work was carried out according to Home Office guidelines in the UK under project license number PPL70/7866. See the Supplemental Experimental Procedures for details.

Statistics

Statistical analysis was done using GraphPad Prism and the Microsoft Office 2016 program package. Paired Student's t test was used to calculate statistical significance. Values of $p < 0.05$ were considered statistically significant. A minimum of three to five animals were used for each experiment.

Microscopy and Imaging

Confocal microscopy used a Leica TCS SP5 system and imaging processing analysis used Leica LAS AF imaging software. For Ring1b and Tunel detection, argon laser 488 nm line excitation and emission maximum at 525 nm were used. For EdU, BrdU, and annexin V excitation, the argon laser 561 nm was used for excitation and, at 617 nm, used as maximum emission. DAPI/Hoechst 33342 was detected using violet (405 nm) laser line and emission maximum at 470 nm. LacZ sections images were obtained on a Zeiss microscope.

DATA AND SOFTWARE AVAILABILITY

The accession number for data reported in this paper is GEO: GSE104893. The SubSeries accession number for the histone ChIPs data reported in this paper is GEO: GSE104891. The accession number for the Ring1b ChIP data reported in this paper is GEO: GSE104892. The accession number for the microarray expression data reported in this paper is GEO: GSE104934.

SUPPLEMENTAL INFORMATION

Supplemental Information includes Supplemental Experimental Procedures, six figures, and three tables and can be found with this article online at https://doi.org/10.1016/j.celrep.2018.05.001.

ACKNOWLEDGMENTS

This study was funded by Medical Research Council grant number MRK018035/1 (to P.S.).

AUTHOR CONTRIBUTIONS

P.T.S. conceived the experiments. Z.A. carried out most of the experiments, analysed the data, and prepared all the figures. B.A. and Y.C. assisted with the Axin2 mice experiment. M.S. and G.Z. assisted with the *in situ* experiment. Z.A. and P.T.S. wrote the manuscript.

DECLARATION OF INTERESTS

The authors declare no competing interests.

Received: October 23, 2017
Revised: February 22, 2018
Accepted: April 25, 2018
Published: June 5, 2018

REFERENCES

An, Z., Sabalic, M., Bloomquist, R.F., Fowler, T.E., Streelman, T., and Sharpe, P.T. (2018). A quiescent cell population replenishes mesenchymal stem cells to drive accelerated growth in mouse incisor. Nat. Commun. *9*, 378.

Aranda, S., Mas, G., and Di Croce, L. (2015). Regulation of gene transcription by polycomb proteins. Sci. Adv. *1*, e1500737.

Bernstein, E., Duncan, E.M., Masui, O., Gil, J., Heard, E., and Allis, C.D. (2006). Mouse polycomb proteins bind differentially to methylated histone H3 and RNA and are enriched in facultative heterochromatin. Mol. Cell. Biol. *26*, 2560–2569.

Biehs, B., Hu, J.K.-H., Strauli, N.B., Sangiorgi, E., Jung, H., Heber, R.-P., Ho, S., Goodwin, A.F., Dasen, J.S., Capecchi, M.R., et al. (2013). BMI1 represses Ink4a/Arf and Hox genes to regulate stem cells in the rodent incisor. Nat. Cell Biol. *15*, 846–852.

Brocardo, M., and Henderson, B.R. (2008). APC shuttling to the membrane, nucleus and beyond. Trends Cell Biol. *18*, 587–596.

Brookes, E., de Santiago, I., Hebenstreit, D., Morris, K.J., Carroll, T., Xie, S.Q., Stock, J.K., Heidemann, M., Eick, D., Nozaki, N., et al. (2012). Polycomb associates genome-wide with a specific RNA polymerase II variant, and regulates metabolic genes in ESCs. Cell Stem Cell *10*, 157–170.

Carpenter, A.C., Rao, S., Wells, J.M., Campbell, K., and Lang, R.A. (2010). Generation of mice with a conditional null allele for Wntless. Genesis *48*, 554–558.

Chiacchiera, F., Rossi, A., Jammula, S., Piunti, A., Scelfo, A., Ordóñez-Morán, P., Huelsken, J., Koseki, H., and Pasini, D. (2016). Polycomb compex PRC1 preserves intestinal stem cell identity by sustaining Wnt/β- catenin transcriptional activity. Cell Stem Cell *18*, 91–103.

Clevers, H. (2006). Wnt/β-catenin signaling in development and disease. Cell *127*, 469–480.

Clevers, H., and Nusse, R. (2012). Wnt/β-catenin signaling and disease. Cell *149*, 1192–1205.

Dietrich, N., Bracken, A.P., Trinh, E., Schjerling, C.K., Koseki, H., Rappsilber, J., Helin, K., and Hansen, K.H. (2007). Bypass of senescence by the polycomb group protein CBX8 through direct binding to the INK4A-ARF locus. EMBO J. *26*, 1637–1648.

Elderkin, S., Maertens, G.N., Endoh, M., Mallery, D.L., Morrice, N., Koseki, H., Peters, G., Brockdorff, N., and Hiom, K. (2007). A phosphorylated form of Mel-18 targets the Ring1B histone H2A ubiquitin ligase to chromatin. Mol. Cell *28*, 107–120.

Enderle, D., Beisel, C., Stadler, M.B., Gerstung, M., Athri, P., and Paro, R. (2011). Polycomb preferentially targets stalled promoters of coding and non-coding transcripts. Genome Res. *21*, 216–226.

Eskeland, R., Leeb, M., Grimes, G.R., Kress, C., Boyle, S., Sproul, D., Gilbert, N., Fan, Y., Skoultchi, A.I., Wutz, A., and Bickmore, W.A. (2010). Ring1B compacts chromatin structure and represses gene expression independent of histone ubiquitination. Mol. Cell *38*, 452–464.

Feng, J., Mantesso, A., and Sharpe, P.T. (2010). Perivascular cells as mesenchymal stem cells. Expert Opin. Biol. Ther. *10*, 1441–1451.

Feng, J., Mantesso, A., De Bari, C., Nishiyama, A., and Sharpe, P.T. (2011). Dual origin of mesenchymal stem cells contributing to organ growth and repair. Proc. Natl. Acad. Sci. USA *108*, 6503–6508.

Frangini, A., Sjöberg, M., Roman-Trufero, M., Dharmalingam, G., Haberle, V., Bartke, T., Lenhard, B., Malumbres, M., Vidal, M., and Dillon, N. (2013). The aurora B kinase and the polycomb protein ring1B combine to regulate active promoters in quiescent lymphocytes. Mol. Cell *51*, 647–661.

Gao, Z., Lee, P., Stafford, J.M., von Schimmelmann, M., Schaefer, A., and Reinberg, D. (2014). An AUTS2-polycomb complex activates gene expression in the CNS. Nature *516*, 349–354.

Juuri, E., Saito, K., Ahtiainen, L., Seidel, K., Tummers, M., Hochedlinger, K., Klein, O.D., Thesleff, I., and Michon, F. (2012). Sox2+ stem cells contribute to all epithelial lineages of the tooth via Sfrp5+ progenitors. Dev. Cell *23*, 317–328.

Kaukua, N., Shahidi, M.K., Konstantinidou, C., Dyachuk, V., Kaucka, M., Furlan, A., An, Z., Wang, L., Hultman, I., Ährlund-Richter, L., et al. (2014). Glial origin of mesenchymal stem cells in a tooth model system. Nature *513*, 551–554.

Kaustov, L., Ouyang, H., Amaya, M., Lemak, A., Nady, N., Duan, S., Wasney, G.A., Li, Z., Vedadi, M., Schapira, M., et al. (2011). Recognition and specificity determinants of the human cbx chromodomains. J. Biol. Chem. *286*, 521–529.

Kondo, T., Isono, K., Kondo, K., Endo, T.A., Itohara, S., Vidal, M., and Koseki, H. (2014). Polycomb potentiates meis2 activation in midbrain by mediating interaction of the promoter with a tissue-specific enhancer. Dev. Cell *28*, 94–101.

Ku, M., Koche, R.P., Rheinbay, E., Mendenhall, E.M., Endoh, M., Mikkelsen, T.S., Presser, A., Nusbaum, C., Xie, X., Chi, A.S., et al. (2008). Genomewide analysis of PRC1 and PRC2 occupancy identifies two classes of bivalent domains. PLoS Genet. *4*, e1000242.

Lapthanasupkul, P., Feng, J., Mantesso, A., Takada-Horisawa, Y., Vidal, M., Koseki, H., Wang, L., An, Z., Miletich, I., and Sharpe, P.T. (2012). Ring1a/b polycomb proteins regulate the mesenchymal stem cell niche in continuously growing incisors. Dev. Biol. *367*, 140–153.

Mi, H., Muruganujan, A., Casagrande, J.T., and Thomas, P.D. (2013). Large-scale gene function analysis with the PANTHER classification system. Nat. Protoc. *8*, 1551–1566.

Moon, R.T., Kohn, A.D., De Ferrari, G.V., and Kaykas, A. (2004). WNT and β-catenin signalling: diseases and therapies. Nat. Rev. Genet. *5*, 691–701.

Pang, Y.W., Feng, J., Daltoe, F., Fatscher, R., Gentleman, E., Gentleman, M.M., and Sharpe, P.T. (2016). Perivascular stem cells at the tip of mouse incisors regulate tissue regeneration. J. Bone Miner. Res. *31*, 514–523.

Pećina-Slaus, N. (2010). Wnt signal transduction pathway and apoptosis: a review. Cancer Cell Int. *10*, 22.

Reya, T., and Clevers, H. (2005). Wnt signalling in stem cells and cancer. Nature *434*, 843–850.

Schwartz, Y.B., and Pirrotta, V. (2008). Polycomb complexes and epigenetic states. Curr. Opin. Cell Biol. *20*, 266–273.

Seidel, K., Ahn, C.P., Lyons, D., Nee, A., Ting, K., Brownell, I., Cao, T., Carano, R.A., Curran, T., Schober, M., et al. (2010). Hedgehog signaling regulates the generation of ameloblast progenitors in the continuously growing mouse incisor. Development *137*, 3753–3761.

Sharpe, P.T. (2016). Dental mesenchymal stem cells. Development *143*, 2273–2280.

Smith, C.E., and Warshawsky, H. (1975). Cellular renewal in the enamel organ and the odontoblast layer of the rat incisor as followed by radioautography using 3H-thymidine. Anat. Rec. *183*, 523–561.

Suzuki, M., Mizutani-Koseki, Y., Fujimura, Y., Miyagishima, H., Kaneko, T., Takada, Y., Akasaka, T., Tanzawa, H., Takihara, Y., Nakano, M., et al. (2002). Involvement of the polycomb-group gene Ring1B in the specification of the anterior-posterior axis in mice. Development *129*, 4171–4183.

Tardat, M., Albert, M., Kunzmann, R., Liu, Z., Kaustov, L., Thierry, R., Duan, S., Brykczynska, U., Arrowsmith, C.H.H., and Peters, A.H.F.M. (2015). Cbx2 targets PRC1 to constitutive heterochromatin in mouse zygotes in a parent-of-origin-dependent manner. Mol. Cell *58*, 157–171.

van Amerongen, R., Bowman, A.N., and Nusse, R. (2012). Developmental stage and time dictate the fate of Wnt/β-catenin-responsive stem cells in the mammary gland. Cell Stem Cell *11*, 387–400.

Wang, X.-P., Suomalainen, M., Felszeghy, S., Zelarayan, L.C., Alonso, M.T., Plikus, M.V., Maas, R.L., Chuong, C.-M., Schimmang, T., and Thesleff, I. (2007). An integrated gene regulatory network controls stem cell proliferation in teeth. PLoS Biol. *5*, e159.

Yang, Z., Balic, A., Michon, F., Juuri, E., and Thesleff, I. (2015). Mesenchymal Wnt/β-catenin signaling controls epithelial stem cell homeostasis in teeth by inhibiting the antiapoptotic effect of Fgf10. Stem Cells *33*, 1670–1681.

Yeo, W., and Gautier, J. (2004). Early neural cell death: dying to become neurons. Dev. Biol. *274*, 233–244.

Yu, T., Volponi, A.A., Babb, R., An, Z., and Sharpe, P.T. (2015). Stem cells in tooth development, growth, repair, and regeneration. Curr. Top. Dev. Biol. *115*, 187–212.

Zang, C., Schones, D.E., Zeng, C., Cui, K., Zhao, K., and Peng, W. (2009). A clustering approach for identification of enriched domains from histone modification ChIP-Seq data. Bioinformatics *25*, 1952–1958.

Zhang, Y., Liu, T., Meyer, C.A., Eeckhoute, J., Johnson, D.S., Bernstein, B.E., Nusbaum, C., Myers, R.M., Brown, M., Li, W., and Liu, X.S. (2008). Model-based analysis of ChIP-Seq (MACS). Genome Biol. *9*, R137.

Zhao, H., Feng, J., Seidel, K., Shi, S., Klein, O., Sharpe, P., and Chai, Y. (2014). Secretion of shh by a neurovascular bundle niche supports mesenchymal stem cell homeostasis in the adult mouse incisor. Cell Stem Cell *14*, 160–173.

Cell Reports, Volume *23*

Supplemental Information

Regulation of Mesenchymal Stem to Transit-Amplifying Cell Transition in the Continuously Growing Mouse Incisor

Zhengwen An, Basem Akily, Maja Sabalic, Guo Zong, Yang Chai, and Paul T. Sharpe

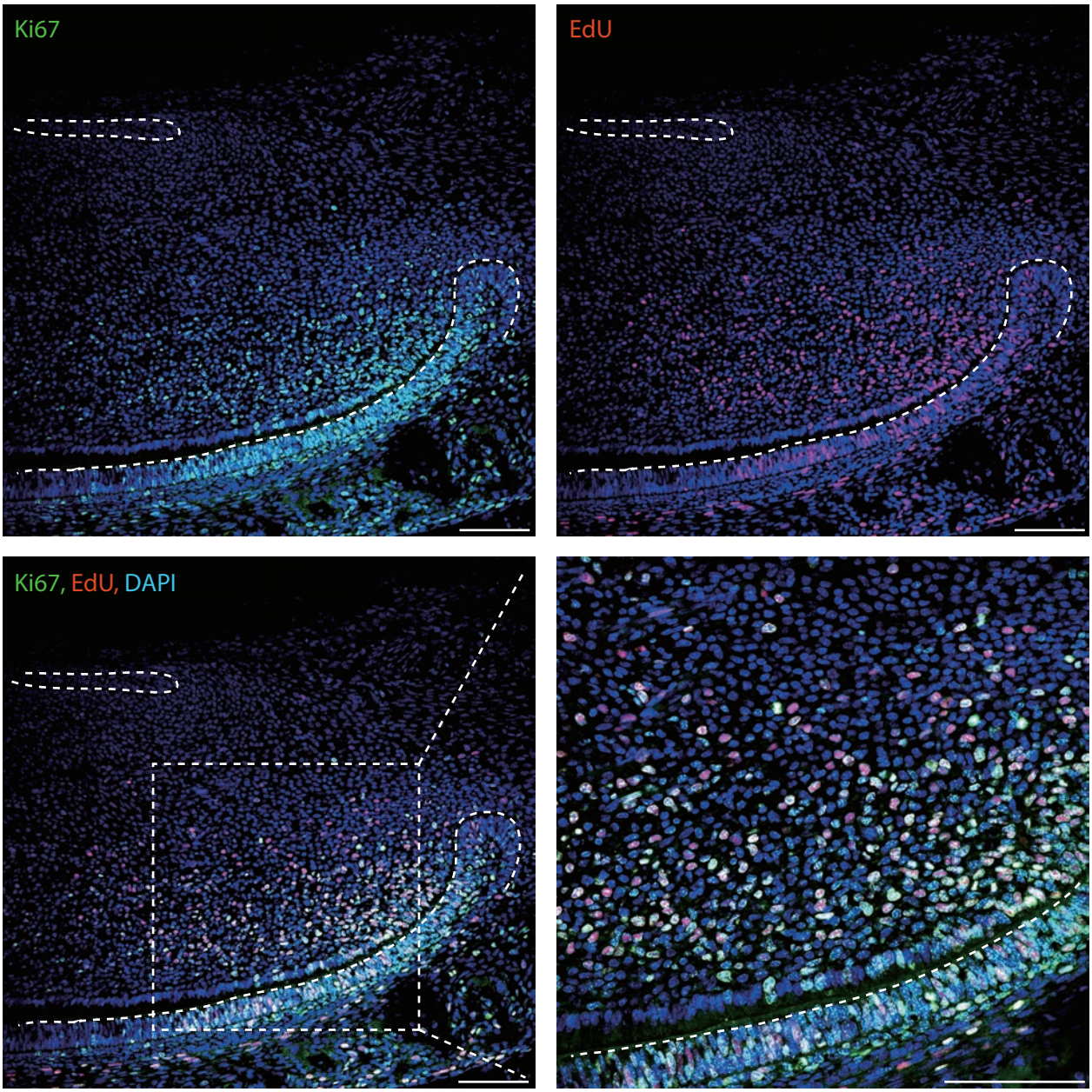

Figure S1. Identification of the TAC region by the cell proliferation marker Ki67 and EdU labelled cells. Related to Figure 1A. Double staining of mouse incisor sagittal sections showing co-localization of Ki67 with 16-24 hours chased EdU+ cells in the TAC region indicative of EdU+ fast cycling TACs. n>=5 mice. Bar is 100 μ m.

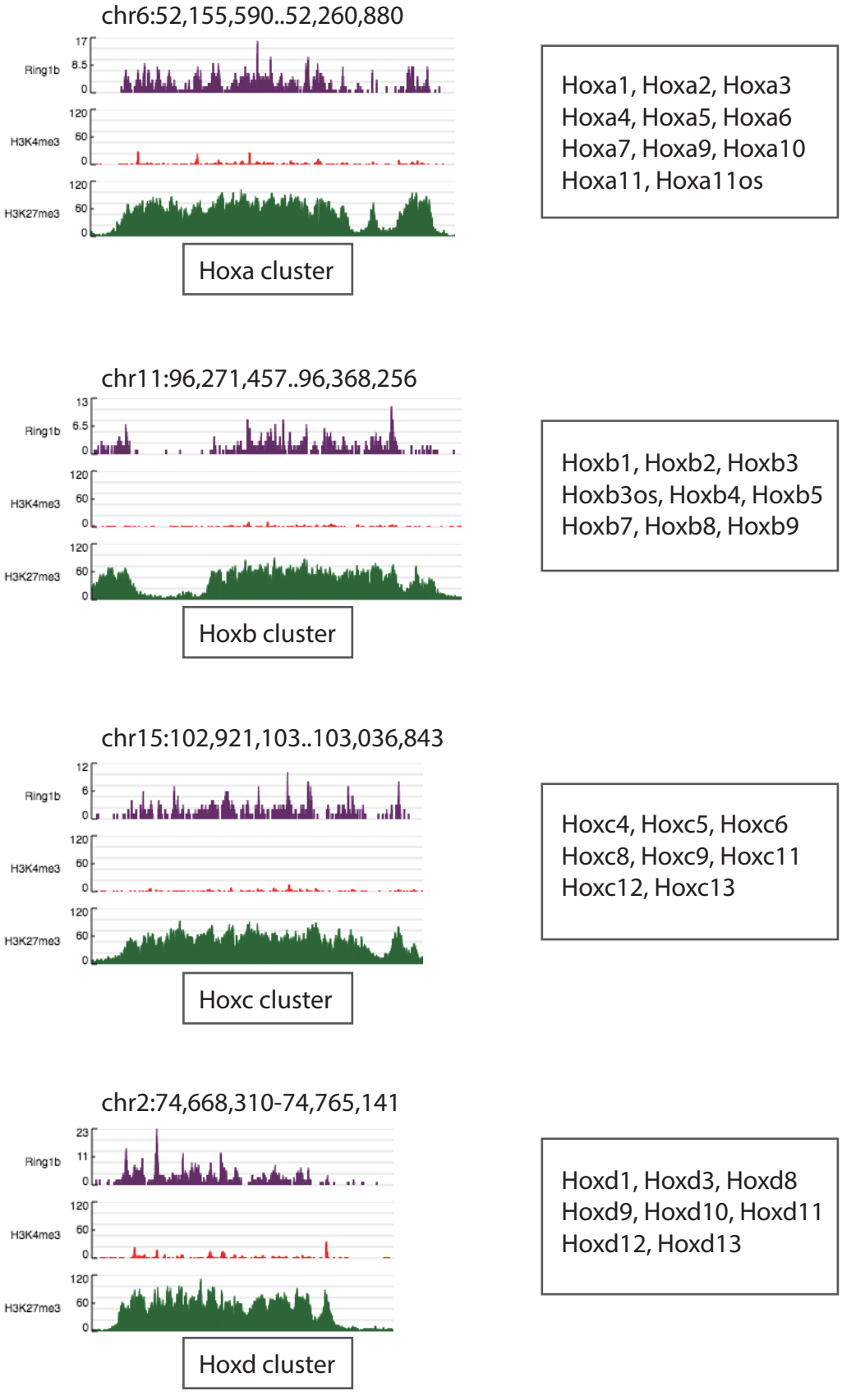

Figure S2. ChIP-seq identifies Hox gene clusters as Ring1b binding loci in TACs. Related to Figure 2A. Genomic views showing Hox clusters co-marked by Ring1b and H3K27me3 but no enrichment with H3K4me3 (left panel). List of Hox genes revealed on ChIP-seq datasets in TACs.

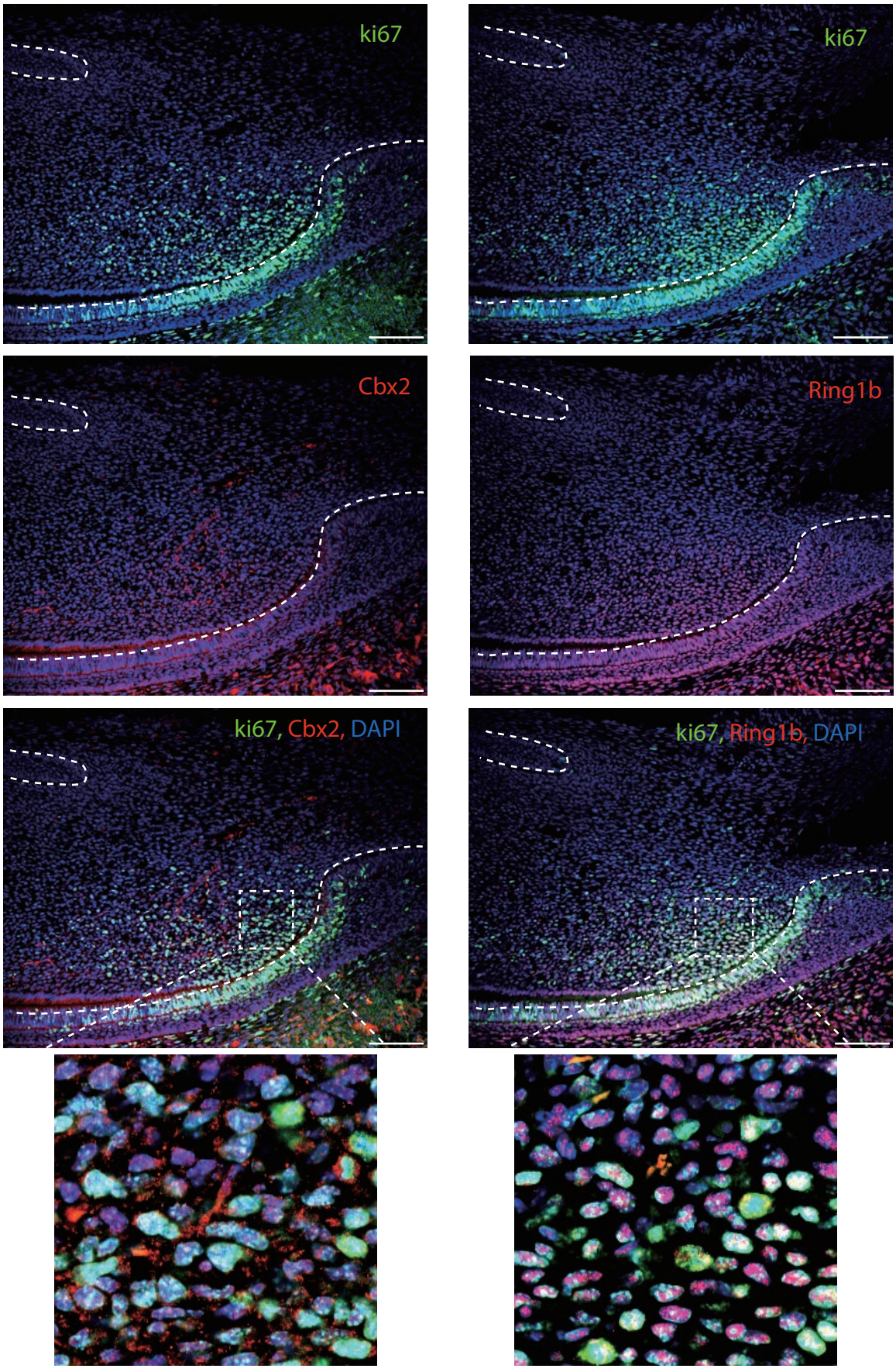

Figure S3. Co-localization of Cbx2 and Ring1b in the mouse dental pulp. Related to Figure 2E-G. Double immuno-staining of Cbx2 and Ring1b both showed co-localization with Ki67 in the TAC region on sequential sections of mouse incisors indicating co-localization of Cbx2 and Ring1b. n>=5 mice per group. Bar is 100 μ m.

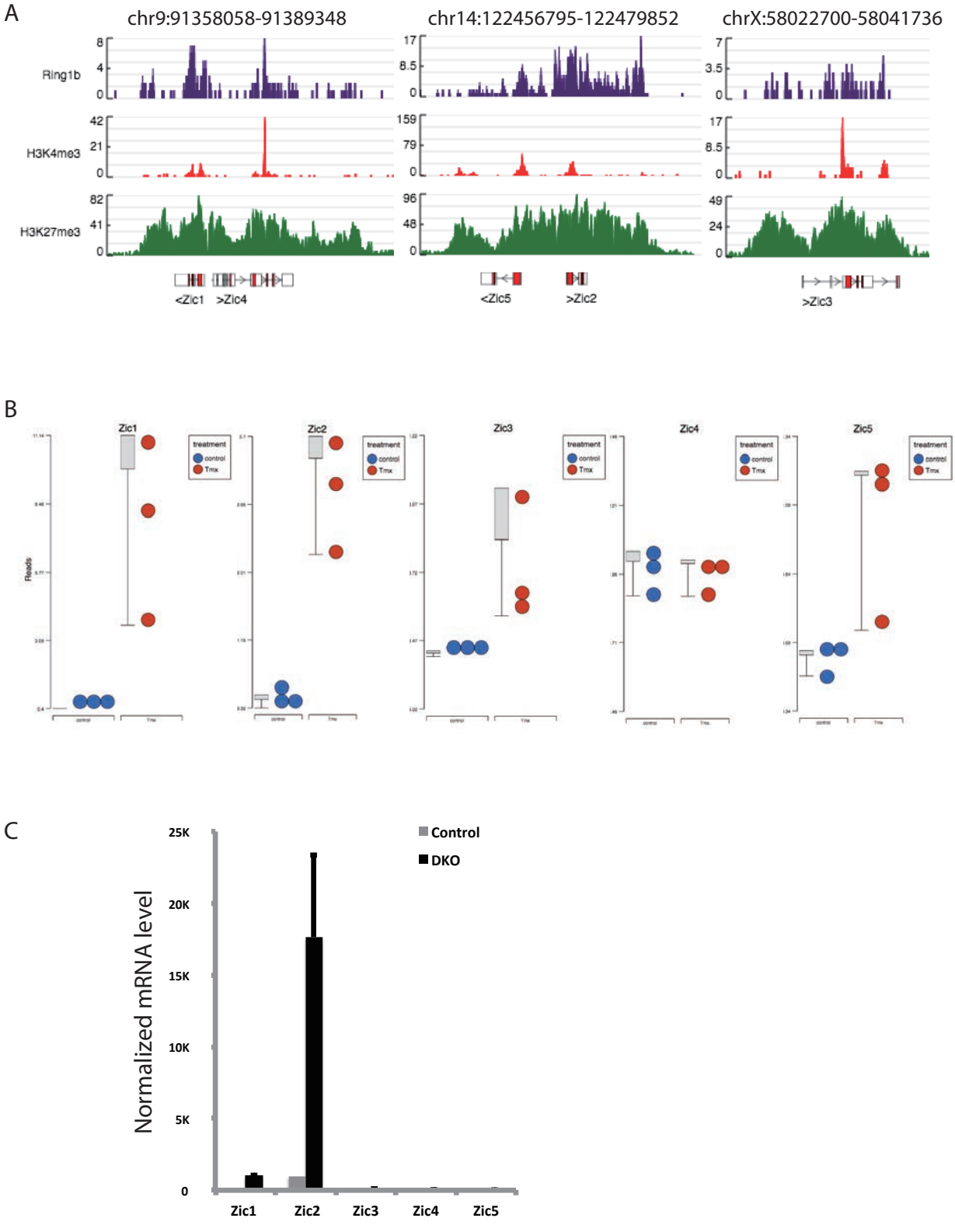

Figure S4. Genomic profiles of Zic family members in TACs. Related to Figure 4E. (A) Genome browser snapshots of Zic1-5 binding profiles. Zic1/2 shows co-occupation with Ring1b and H3K27me3, while other Zic family members also showed binding with H3K4me3. (B) Dot plots showed only Zic1/2 significantly up-regulated following deletion of Ring1b (n=3, $P<0.05$), whereas Zic3, Zic4 and Zic5 showed no significant difference (n=3, $P>0.05$) on microarray datasets. (C) Validation of Zic expression following loss of Ring1b by qPCR confirmed that Zic1/2 were significantly up-regulated compared with other Zic family members (n>=3, $P<0.001$ by Student's t-test). Data presented as mean ± S.E.M.

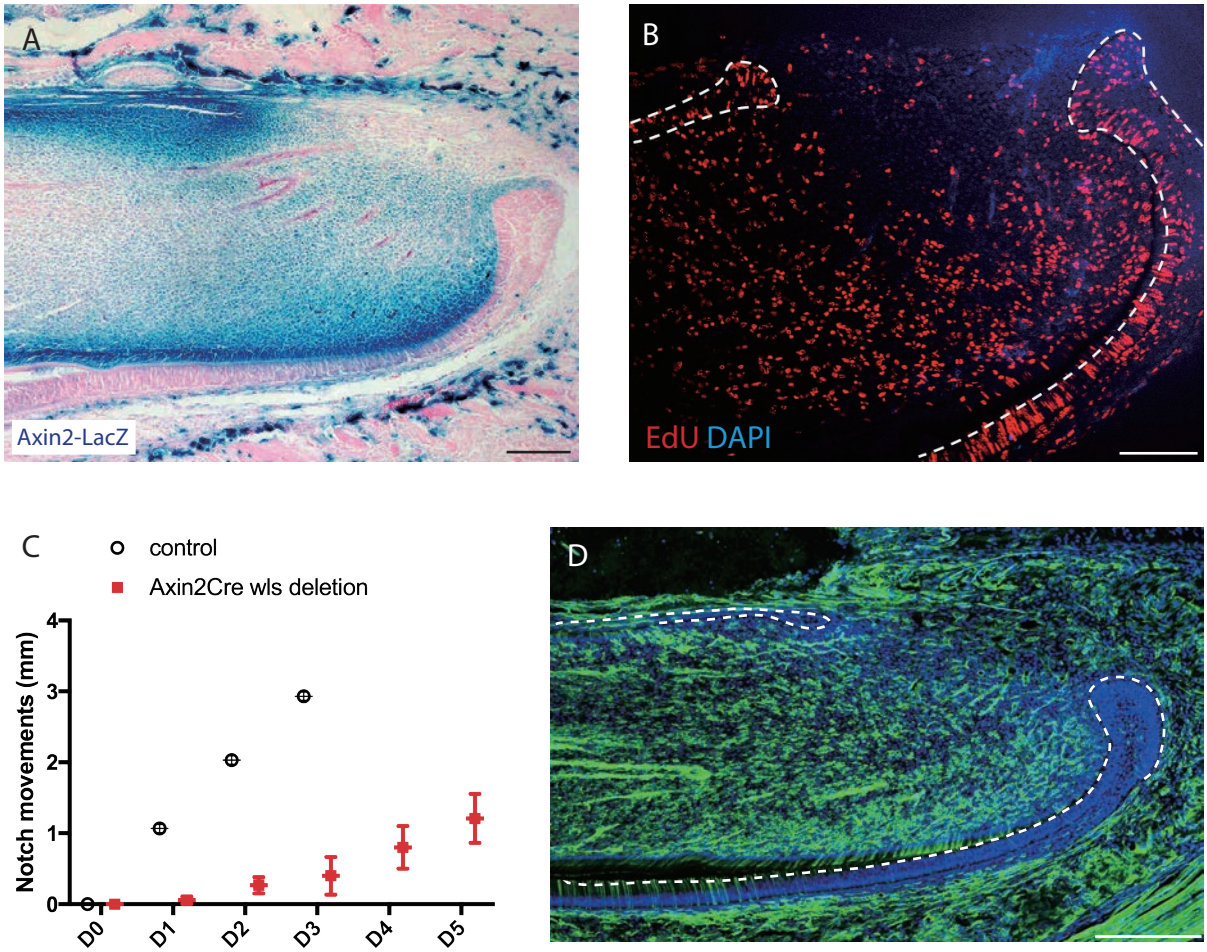

Figure S5. Axin2 expressed in TACs in the mouse incisor. Related to Figure 5 and Figure 6D.
(A) Sagittal section of Axin2LacZ mouse incisor stained for beta-galactosidase (LacZ) activity using X-gal showing Axin2 expression in the TAC region. (B) EdU+ cells detected in the TAC region after 16-24 hours chasing. n>=5 mice. (C) Comparison of growth rates. After one week of three doses of tamoxifen, notches were made 0.8-0.9 mm above the incisor gingiva at day 0 (D0) in Axin2cre;wls cko/cko and control mice. Notch movements were measured every day for five days. Notches in control incisors reach the tip after 3 days, while the notches in Axin2cre;wls cko/cko incisors only reach about 1/3 of full length incisor by day 5. n=3 and P<0.01 by Student's t-test. (D) Efficiency of Cre recombinase in the mouse incisor. PcagCreERT2 mice crossed with the mTmG reporter mouse line. Mouse incisors were harvested after two doses of tamoxifen (5 mg/30 g body weight) showed widespread location of GFP+ cells in mesenchyme. n=4 mice. Bar is 250 μ m.

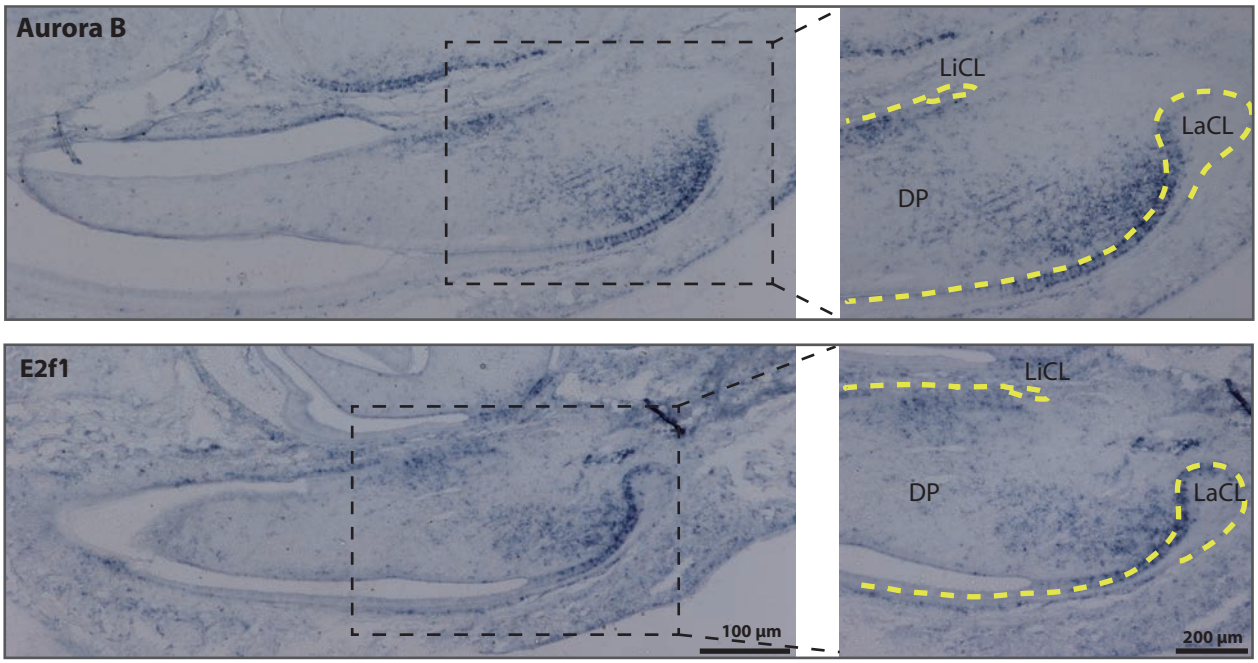

Figure S6. In situ hybridisation identifies Aurora B and E2f1 in TACs. Related to Figure 3E.
Aurora B and a positive cell cycle regulator E2f1 are detected mainly in the incisor mesenchyme between the labial and lingual aspects of the cervical loop where TACs are located. n>=3 mice per group. DP is for Dental Pulp, LiCL is for Lingual Cervical Loop and LaCL is for Labial Cervical Loop.

Table S2. List of real-time PCR primers. Related to Figure 3I, 3J and Figure 4D, 4F.

Primer name	Primer sequencing
Axin2-Forward	gagagtgagcggcagagc
Axin2-Reverse	cggctgactcgttctcct
Beta-actin-Forward	ctaaggccaaccgtgaaaag
Beta-actin-Reverse	accagaggcatacagggaca
Beta-catenin-Forward	ttcctatgggaacagtcgaag
Beta-catenin-Reverse	ttgtattgttactcctcgaccaaa
Cdc6-Forward	ctgtttcaggagacatccgtaa
Cdc6-Reverse	tcctgacatccgactccac
Cdc7-Forward	gcggacgtcctaacttctgt
Cdc7-Reverse	gcttccactacgcacgact
Cdc45-Forward	ggcaagaacttgaaactgcat
Cdc45-Reverse	cactggcctgtgggtatca
Cdkn2a-Forward	cgtaccccgattcaggtg
Cdkn2a-Reverse	accagcgtgtccaggaag
CyclinD1-Forward	tttctttccagagtcatcaagtgt
CyclinD1-Reverse	tgactccagaagggcttcaa
CyclinE2-Forward	cgagctgtggagggtctg
CyclinE2-Reverse	aaacggctactgcgtcttga
E2f1-Forward	tgccaagaagtccaagaatca
E2f1-Reverse	cttcaagccgcttaccaatc
Myc-Forward	cctagtgctgcatgaggaga
Myc-Reverse	tccacagacaccacatcaattt
Twist1-Forward	agctacgccttctccgtct
Twist1-Reverse	tccttctctggaaacaatgaca
Zic1-Forward	aacctcaagatccacaaaagga
Zic1-Reverse	cctcgaactcgcacttgaa
Zic2-Forward	gatccacaaaagaactcatacagg
Zic2-Reverse	cttcttcctgtcgctgctgt
Zic3-Forward	cctgcgcaaacacatgaa
Zic3-Reverse	ctatagcgggtggagtggaa
Zic4-Forward	gtggagcagggctcaaac
Zic4-Reverse	tggtgtccacagctgctact
Zic5-Forward	cactgccaccaacagtgg
Zic5-Reverse	aggacgaagtccctgctgt

Table S3. Plasmids used for Digoxigenin-labelled RNA probes. Related to Figure S6.

Name	Vector	5' clone site	3' clone site	Anti-sense probe	Sense probe	IMAG ID
Aurora B	pT7T3D-PacI	EcoRI	NotI	T3	T7	1226941
E2f1	pSPORT1	SalI	NotI	Sp6	T7	934181

Supplemental Experimental Procedures:

EdU / BrdU incorporation and staining

EdU was detected by Click-iT EdU Alexa Fluor 647 Imaging kit (Invitrogen C10340) according to the protocol. BrdU was detected by anti-BrdU antibody (ab6326, Abcam) 1:100 followed by secondary antibody donkey anti-Rat IgG (H+L) Alexa Fluor 594 (Invitrogen) 1:400 prior to DAPI staining for nuclei and cover-slipped for microscopy.

Immunofluorescence

Immunofluorescence staining used standard protocols on 12 µm sagittal cryosections of mouse incisors. Anti-mouse Ring1b antibody (Active motif #39663, 1:100), anti-Rabbit Ring1b (ab101273, Abcam, 1:500), anti-Rabbit Ki67 antibody (Abcam ab15580, 1:100) and anti-Rabbit CBX2 antibody (Abcam ab184968, 1:100) were used as primary antibodies. Goat anti-mouse IgG (H+L) Alexa Fluor 488, Donkey anti-rabbit IgG (H+L) Alexa Fluor 488, Alexa Fluor 594 and Alexa Fluor 647 (invitrogen, 1:400) were used as secondary antibodies. Hoechst 33342 (Invitrogen 62249, 1:500) used for DNA staining. Slides were then mounted using glycerol based antifade Citifluor™ AF1 (Citifluor Ltd., AF1-100) and cover slips added.

Cytospin

Flow sorted EdU+ cells were collected and re-suspended as 100 µl aliquots in 2% BSA in PBS before loading into a Shandon Single Cytofunnel. Cells were then forced to separate and deposited as a monolayer on slides to preserve the cellular integrity using Shandon Cytospin 3 Centrifuge at 1350 rpm for 5 minutes. Slides were then post-fixated, permeablized and immunostained with primary and secondary antibodies followed by DNA staining with Hoechst33342 prior to coverslips being added according to the standard protocol.

ChIP seq

Primary incisor pulp cells were isolated from 80 incisors for each set of ChIP-Seq. Cells were cross-linked with 1% formaldeyde at room temperature for 12 minutes and then quenched with 0.125 M glycine for another 5 minutes. Cells were suspended in 100 µl saponin-based permeablization buffer and labelled EdU by Click-iT® EdU Alexa Fluor® 647 Flow Cytometry Assay Kit (Thermo Fisher Scientific, C10424). FACS sorted EdU+ cells were collected and sonicated to yield chromatin at 100-500bp. Low-input ChIP was performed by

standard procedures using antibodies from Active motif (Ring1b antibody, 39663; H3K4me3, 39915; H3K27me3, 39155).

Two replicate ChIPseq experiments for Ring1b were pooled for the input sample. Total number of reads were over 40 million for each ChIPseq. The unique alignments without duplicate reads (final tags) were less than 1 million for Ring1b ChIPseq. Peaks were determined using the MACS peak finding algorithm. Using a cutoff of p-value = 1e-6, 3938 peaks were identified. A total of 6.2 million final tags were obtained for H3K4me3 and 13.6 million for H3K27me3. Peaks were determined using the SICER algorithm at a cutoff of E-value = 1 and a Gap parameter of 600 bp. 14,361 H3K4me3 enriched regions and 11,341 H3K27me3 enriched regions were identified respectively.

Western blots

Mouse incisor pulp tissues were disrupted by a hand rotor homogenizer and protein was extracted using cell lysis buffer (CLB) (10 mM Tris pH8.0, 10 mM NaCl, 0.2%NP40) followed by nuclear lysis buffer (NLB) (50 mM Tris pH8.1, 10 mM EDTA, 1%SDS). Equal volume of 2x SDS loading buffer (100 mM TrisHCL PH6.8, 4% SDS, 12% Glycerol, 2% β-mercapitalethanol, 0.008% bromophenol blue) was added to 30µg protein followed by incubation at 95° C for 3 minutes before loading onto SDS-PAGE gels and wet transfer to nitrocellulose membranes. Anti-Ring1b (Active motif 39663, 1:500) and anti-H3K27me3 antibodies (Diagenode pAb-069-050, 1:500) were used to detect protein expression levels and anti-Lamin B1 antibody (Abcam, Ab16048, 1:1000) used as an internal loading control. Peroxidase-conjugated Affinipure Goat-anti Rabbit IgG (H+L) (Jackson immunoResearch, 111-035-003, 1:3000) and Peroxidase-conjugated Affinipure Goat-anti mouse IgG (H+L) (Jackson immunoResearch 111-035-003, 1:3000) were used as secondary antibodies against primary antibodies prior to ECL (GE Healthcare Life Science, RPN2232) detection.

Co-immunoprecipitation

Protein was extracted from mouse incisor pulp tissue using RIPA buffer (150 mM NaCl, 1.0% NP-40, 0.5% sodium deoxycholate, 0.1% SDS and 50 mM Tris, pH 8.0) supplemented with protease inhibitor cocktail (Roche). The protein extract was precleared with 35 µl protein A/G Plus-Agarose beads (Santa Cruz, sc-2003) and immunoprecipitated with 3µg antibody of anti-H3K27me3 (Diagenode, pAb-069-050), anti-H2AK119ub (Cell signalling, #8240), anti-Ring1b (Active motif, 39663), 3µg anti-mouse IgG (PEPROTECH, 500-M00) was used as a

control, together with 35 µl protein A/G Plus-Agarose beads incubated at 4° C for 2 hours on a rotator. Beads were pelleted by centrifuge at 13000 rpm for 1minute. Equal volume of 2x SDS loading buffer (100 mM TrisHCL PH6.8, 4% SDS, 12% Glycerol, 2% β-mercaptoethanol, 0.008% bromophenol blue) was added to the bead pellets and protein complexes were eluted by incubation at 95° C for 3 minutes before loading onto SDS-PAGE gels and wet transfered to nitrocellulose membranes. Primary antibody anti-Ring1b and secondary antibody Peroxidase-conjugated Affinipure Goat-anti mouse IgG (H+L) were used to detect the interaction proteins in the precipitated protein complex followed by ECL detection.

Quantitative Real-time PCR

Total RNA was extracted from mouse dental pulp tissue using RNeasy Mini Kit (Qigen 74104), and purified by Ambion DNA-free DNA Removal Kit (Invitrogen, AM1906). cDNA was then synthesised using MMLV Reverse Transcriptase (Promega, 9PIM170). Both cDNA without MMLV reverse transcriptase and RNase-free water with MMLV reverse transcriptase were used as negative controls. For each sample, 1 µg cDNA was used for qPCR reaction with the LightCycler 480 SYBR Green I Master (Roche, 04707516001) using LightCycler 480 system qPCR platform (Roche, 05015278001). All primers used in the experiments are listed in Table S2. Data were analysed with $2^{-\Delta\Delta ct}$ methods. All ct values were normalized with β-actin levels as internal controls. Standard deviations were calculated from biological triplicate samples and were represented as error bars.

Cryosection preparation

Moue incisor samples were fixed in 4% PFA in PBS for 24-48 hours at 4° C and decalcified in 10-19% EDTA for 4 weeks. Samples were then sucrose cryoprotected by incubation with 30% sucrose until samples sunk to the bottom followed by incubation with half of 30% sucrose and half of OCT compound (VWR, 361603E) before embedding in OCT. Cryosectioning of samples at 10-12 um thickness was carried by Cryostat Microtome (Bright, OTF5000). Sections were stored at -80 ° C prior to staining.

LacZ staining

Frozen sections were post-fixed in 0.2% glutaraldehyde and permeabilized in 0.05% Tween20 (Sigma Aldrich) in PBS and then incubated in X-gal solution (Thermo scientific) overnight at 37° C for LacZ staining. Fast red was used for counterstaining.

Tunel assay

Frozen incisor sections were post-fixed in 4% PFA then permeabilized in 0.1M Sodium Citrate buffer with PH 6.0 (11.5% 0.1M citric acid monohydrate and 88.5% 0.1M Trisodium Citrate dihydrate) on ice. The sections were incubated in Tunnel reaction mixture at 37° C for 60 minutes according to the protocol (In Situ Cell Death Detection Kit, Fluorescein 11684795910 Roche) and counterstained with Hoechest33342 prior to coverslip. Fluorescein was detected by Confocoal microscopy (Leica TCS SP5) with an argon laser at 488nm excitation.

Digoxigenin-labelled section in situ hybridization

In situ hybridization (ISH) for detection of mouse Aurora B and E2f1 mRNA expression was performed on 12 μm cryo-sections of mouse incisors following the standard procedures. Briefly, 10 μg plasmid (Table S3) was linearized by 5' and 3' clone site restriction enzymes for sense and anti-sense probes. 1μg linearized DNA was used for DIG-labelling (Roche) and RNA probes were synthesised at 37° C for 2 hours followed by 2 μl DNase I incubation for 15 minutes at 37° C. Probes were then purified by SigmaSpin post-Reaction Clean-up Colums (S0185-70EA). Sections were fixed in 4% paraformaldehyde and hybridized with 1μl digoxigenin-labelled sense and antisense probes. Sections were treated with RNase-A or treated with the sense probe are used as negative controls. Images were taken on a Zeiss Axioskop 2 microscope equipped with a Zeiss AxioCam camera (Carl Zeiss).

Mice information

Wild type CD1 mice were obtained from CRL (Charles River Laboratory, UK). Mutant Ring1a and Ring1b floxed alleles were generated as described previously (Lapthanasupkul et al., 2012; Cales et al., 2008; and del Mar Lorente et al., 2000). $Ring1a^{-/-}$;$Ring1b^{fl/fl}$ compound mice were crossed with $pCAG^{CreERT2}$ transgenic mice to generate Ring1a-/-;Ring1bfl/fl ;Rosa26::CreERT2 mice. Ring1a-/-;Ring1bcko/cko mice were obtained by injecting 4-hydroxy tamoxifen (OHT) (40mg/kg body weight) and corn oil as control for 2 days before being scarified.

Axin2CreERT2/+ mouse line was described previously (Van Amerongen et al, 2012). A total of 14 mice were divided into 4 groups and Cre recombination was activated by 3 doses of Tamoxifen (Sigma Aldrich) injections (5 mg/30 g body weight) and corn oil as control. Mice then collected at 1, 3, 7, 14 and 28 days following the last injection of tamoxifen.

Ubiquitous $Pcag^{CreERT2}$ mouse line was crossed with $Wls^{fl/fl}$ mouse line (Carpenter et al, 2010). A total of 6 mice were divided in to 2 groups. The first group were treated with 3 doses of tamoxifen injections to activate cre recombination. The other groups were treated with 3 doses of corn oil injections as control. Both groups were collected 7 days post injection. Cre activity was analysed by crossing $Pcag^{CreERT2}$ with the R26R-mTmG reporter mice (Figure S5).